GSA Data Repository 2014134

Evidence for a Noachian-aged ephemeral lake in Gusev crater, Mars

Steven W. Ruff[1], Paul B. Niles[2], Fabrizio Alfano[1], and Amanda B. Clarke[1]
[1]*School of Earth and Space Exploration, Arizona State University, Tempe, AZ 85287, USA*
[2]*Astromaterials Research Exploration Sciences, NASA Johnson Space Center, Houston, TX 77058, USA*

ITEM DR1. DETAILED METHODS

DR1.1. Spectral Unmixing

Linear least squares unmixing (Ramsey and Christensen, 1998) of the Mini-TES spectrum from the Comanche outcrop target named Saupitty (sol 701, product ID P3340) employed the same library of laboratory mineral spectra as that used previously (Morris et al., 2010) with the exception of the inclusion of an average of the six Algonquin spectra shown in Fig. 2a and the spectrum of synthetic olivine with Fo_{75} composition (Lane et al., 2011). In addition to mineral phases, the library included spectra representing both optically thick and thin martian dust (Hamilton and Ruff, 2012), a "slope" spectrum to account for any temperature determination errors (Ruff et al., 2006), and a blackbody spectrum to account for differences in spectral contrast between the laboratory and Mini-TES spectra. Following previous practice *(Ruff et al., 2006)*, the spectral range used in the calculations (~380 to 570 cm-1 and ~780 to 1350 cm-1) excludes contributions from atmospheric CO_2 and the noisiest portions of the Mini-TES spectra. The results of the calculations are normalized to the mineralogic endmembers to give their relative contribution to the spectrum (i.e., area % of the target) (Table DR1).

The spectral mixture of carbonate phases is recognizable as a broadening of a feature near 900 cm^{-1} compared with that of a single composition carbonate (Fig. 2a). This broadening better fits the counterpart feature in the Comanche spectrum and arises from mixing of the ν_2 feature (out-of-plane bend of the C-O bond) of multiple carbonates, which shifts with composition (Lane and Christensen, 1997). A mixture of carbonates also better fits a narrow peak near 475 cm^{-1} in the Comanche spectrum, where an adjacent, wider peak in olivine is subdued when spectrally mixed with carbonates (Fig. 2b).

The modeled amorphous silicate component represents a spectrum of natural Hawaiian basaltic glass that displays incipient alteration akin to opal-A. The sample and spectrum were provided by R.V. Morris.

DR1.2. Chemical Modeling

Elemental data from Alpha Particle X-Ray Spectrometer (APXS) measurements of Comanche and Algonquin (Ming et al., 2008; Morris et al., 2010) were modeled as chemical gains and losses in two different ways. The first utilized a mass balance model from a previous study (Amundson et al., 2008) where Ti composition can be used as an index for ascertaining the amount of relative chemical addition or subtraction made to a material assuming that an

appropriate pre-cursor material (or parent) can be identified. In this case we assume that Algonquin chemistry (Ming et al., 2008) resembles that of Comanche Palomino before the alteration that resulted in carbonate formation. This method also assumes that Ti remains immobile and therefore ratios of elements to Ti reveal absolute additions or subtractions. The molar gains and losses were calculated according to the formula:

$$(\text{Moles Gain/Loss per 100g}) = X_C - X_A*(Ti_C/Ti_A) \quad (1)$$

where X_C is the number of moles of element x in Comanche, X_A is the number of moles of element x in Algonquin, Ti_C is the number of moles of Ti in Comanche, and Ti_A is the number of moles of Ti in Algonquin. In all cases the number of moles is calculated based on 100 g of sample. Results of these calculations clearly indicate significant additions of Mg, Fe, and Si, with little to no change of any other elements (Fig. 3a).

The second method for addressing chemical gains and losses is through a simple component analysis in which the Comanche composition is modeled as a two-component mixture of an Algonquin-like precursor plus an alteration component (Table DR2). By subtracting a fractional amount of the Algonquin composition sufficient to remove all of the TiO_2 from the starting Comanche composition, the alteration component can be determined. Subtracting 63% of Algonquin removes TiO_2 and essentially zeros out the molar abundance of Na_2O, Al_2O_3, P_2O_5, and Cr_2O_3 as well, demonstrating the insensitivity of the method to the assumed immobile element. The remaining chemistry attributable to the alteration very closely resembles that calculated from the mass balance model described above (Fig. 3a). This provides a robust indication that the alteration of Comanche is due to the addition of Mg, Fe, and Si-rich phases to an Algonquin-like host.

Using GEOCHEQ thermochemical modeling (Mironenko et al., 2008), we investigated the composition of fluids in equilibrium with a rock of Algonquin composition under a range of conditions, similar to the approach used by Niles et al. (2009) to model the fluids that produced the carbonates in ALH 84001. A CO_2 atmosphere at 100 mbars partial pressure, a water-to-rock (W/R) ratio of 10^5, temperature of 25 or 50° C, and pH in the 5-6 range results in enrichments of Fe^{2+}, Mg^{2+}, SiO_2, and HCO_3^- proportional to the additions recognized from the mass balance modeling (Fig. 3). Lower temperatures are required due to the decreasing solubility of CO_2 with increasing temperature as well as the decreasing Fe^{2+} content due to decreased solubility of iron oxides with increasing temperature. The high W/R value represents a relatively dilute solution based on short-lived water-rock interaction. Limited amounts of solid goethite and kaolinite are present in the final calculation, but the fluid composition closely resembles that observed as chemical additions in the mass balance modeling. Lower W/R ratios did not yield fluids with similar chemical concentrations as the calculated additions to Comanche, due to precipitation of secondary phases.

DR1.3. Textural Analysis

Textural characteristics of the Comanche and Algonquin outcrops were determined through image analysis of two MI mosaics of the brushed targets Palomino and Iroquet, respectively. The images were processed using Photoshop PS3, drawing the particle outline

where it was possible to identify with confidence (Fig. DR1). The main challenge arose from the rough surfaces present in the images and consequent shadows, most notable on the Comanche Spur Palomino target. Our general approach was to consider only the particles with a clear and identifiable outline. Where a shaded area was present, the outline of the clear portion and the outline of the shaded portion were drawn and the ratio between the two surfaces was calculated. Only those particles with the percentage of shaded portion less than the 25% of the whole particle outline were considered. As the image processing was completed, and binary images were produced, they were analyzed using Jmicrovision 1.2.7 (http://www.jmicrovision.com/) to determine the area, the equivalent circular diameter, width and length (the shortest and longest dimension, respectively) of each particle.

The observed particle size distribution (expressed in a logarithmic scale commonly used in sedimentology; $\Phi = -\log_2$ diameter) shows the range of dimensions of the particles that were identifiable (Fig. DR2). The distribution appears to be similar for the two outcrops, and differs only in that the particle sizes of the Algonquin outcrop are slightly smaller. However, both outcrops are well sorted, presenting a small standard deviation (σ_Φ is 0.6 and 0.5 for Comanche and Algonquin respectively) that is typical of fall-out deposits. The second plot (Fig. DR2) shows the aspect ratio distribution (ratio between width and length) for the two outcrops. The distributions are fairly similar, suggesting that the particles were subjected to a similar sedimentation regime. The relatively high degree of elongation indicates a limited or nearly absent horizontal transport along the ground.

ITEM DR2. EXTENDED RESULTS

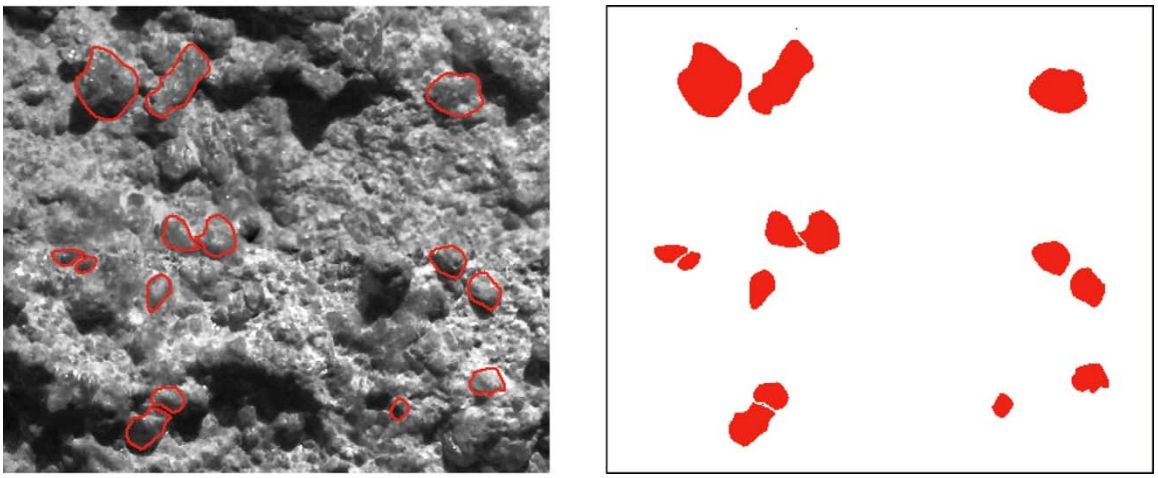

Figure DR1. Example of the textural analysis applied to images from the MI. The view on the left shows a ~1 cm wide portion of the brushed surface on the target Palomino on Comanche Spur. Red outlines enclose examples of identified particles, which are shown in the binary image on the right [Credit: NASA/JPL/USGS].

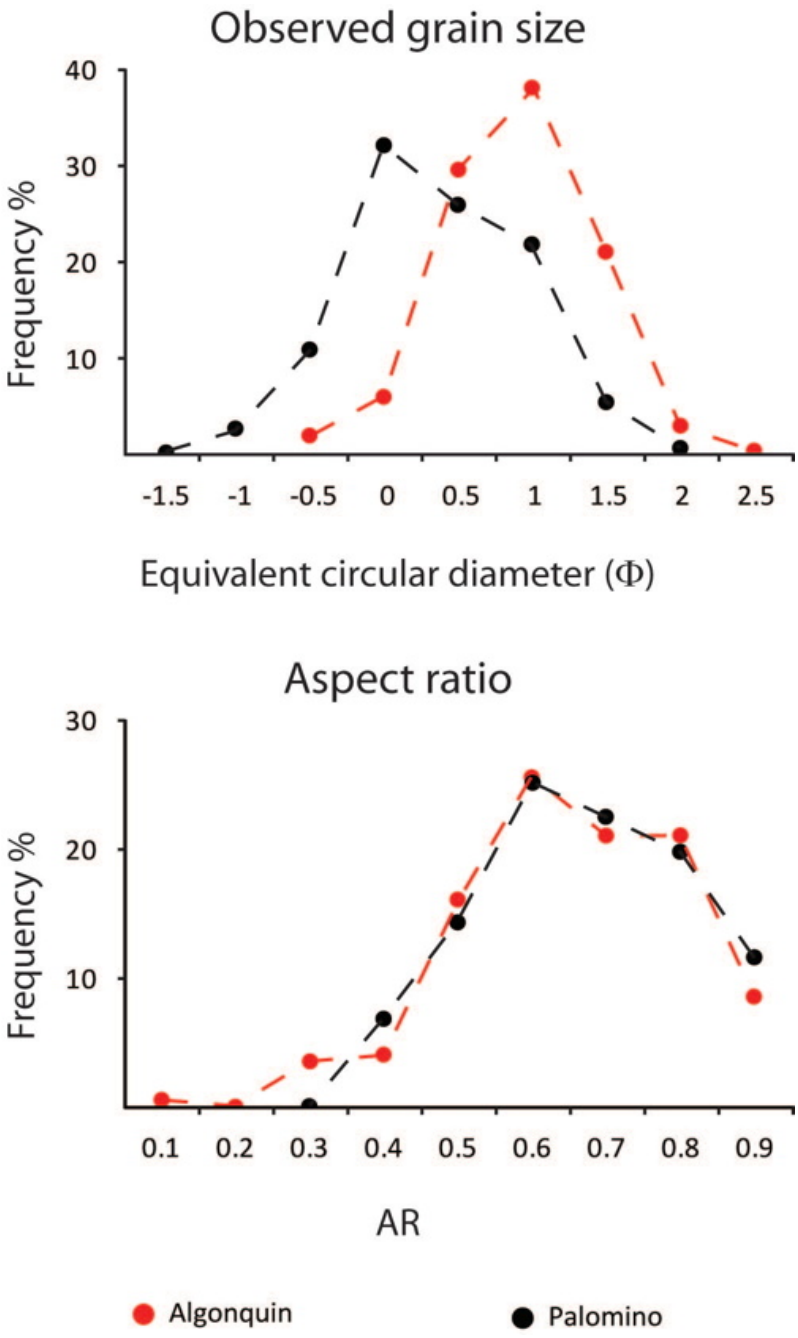

Figure DR2. Results of analysis of the outcrop images. The upper plot presents the size distribution and the lower plot shows the aspect ratio of particles identified in MI images of the two outcrops.

Table DR1. Spectral components derived from linear least squares unmixing of the Mini-TES spectrum of the Comanche Saupitty target, presented as area percent.

Component	Complete (%)	Normalized (%)
Average Algonquin	27	73
Amorphous silicate	3	9
Mg-Fe carbonate	3	7
Siderite	2	6
Magnesite	2	5
Optically thick dust	3	0
Blackbody	61	0
Total	100	100

Table DR2. Results of a two-component model of Comanche Spur Palomino APXS chemistry. After subtracting 63% of Algonquin to remove all the TiO_2 from Comanche, the remaining alteration component is enriched in Mg, Fe, and Si.

	Comanche[1] (moles)	Algonquin[2] (moles)	Alteration (moles)
Na_2O	0.016	0.016	0.000
MgO	0.536	0.349	0.187
Al_2O_3	0.025	0.025	0.000
SiO_2	0.601	0.426	0.175
P_2O_5	0.003	0.003	0.000
SO_3	0.029	0.034	-0.005
Cl	0.015	0.015	-0.001
K_2O	0.000	0.001	0.000
CaO	0.030	0.029	0.001
TiO_2	0.003	0.003	0.000
Cr_2O_3	0.004	0.004	0.001
MnO	0.005	0.003	0.002
FeO_T	0.275	0.186	0.089
CO_2	0.273	0.000	0.273
Total	1.816	1.093	0.722
Mass	100g	63g	37g

[1]From (Morris et al., 2010)
[2]From (Ming et al., 2008)

REFERENCES CITED

Amundson, R., Ewing, S., Dietrich, W., Sutter, B., Owen, J., Chadwick, O., Nishiizumi, K., Walvoord, M., and McKay, C., 2008, On the in situ aqueous alteration of soils on Mars: Geochimica et Cosmochimica Acta, v. 72, p. 3845–3864, doi:10.1016/j.gca.2008.04.038.

Hamilton, V.E., and Ruff, S.W., 2012, Distribution and characteristics of Adirondack-class basalt as observed by Mini-TES in Gusev crater, Mars and its possible volcanic source: Icarus, v. 218, no. 2, p. 917–949, doi:10.1016/j.icarus.2012.01.011.

Lane, M. D., and Christensen, P. R., 1997, Thermal infrared emission spectroscopy of anhydrous carbonates.: J. Geophys. Res., v. 102, p. 25,581-525,592.

Lane, M.D., Glotch, T.D., Dyar, M.D., Pieters, C.M., Klima, R.L., Hiroi, T., Bishop, J.L., and Sunshine, J., 2011, Midinfrared spectroscopy of synthetic olivines: Thermal emission, specular and diffuse reflectance, and attenuated total reflectance studies of forsterite to fayalite: Journal of Geophysical Research, v. 116, no. E08010, doi:10.1029/2010JE003588.

Ming, D. W., Gellert, R., Morris, R. V., Arvidson, R. E., Bruckner, J., Clark, B. C., Cohen, B. A., d'Uston, C., Economou, T., Fleischer, I., Klingelhofer, G., McCoy, T. J., Mittlefehldt, D. W., Schmidt, M. E., Schroder, C., Squyres, S. W., Treguier, E., Yen, A. S., and Zipfel, J., 2008, Geochemical properties of rocks and soils in Gusev Crater, Mars: Results of the Alpha Particle X-Ray Spectrometer from Cumberland Ridge to Home Plate: Journal of Geophysical Research, v. 113, no. E12S39, doi:10.1029/2008JE003195.

Mironenko, M. V., Melikhova, T. Y., Zolotov, M. Y., and Akinfiev, N. N., 2008, GEOCHEQ_M: Program complex for thermodynamic and kinetic modeling of geochemical processes in rock-water-gas systems. Version 2008: Herald DGGGMS RAS, v. 1, no. 26.

Morris, R.V., Ruff, S.W., Gellert, R., Ming, D.W., Arvidson, R.E., Clark, B.C., Golden, D.C., Siebach, K., Klingelhöfer, G., Schröder, C., Fleischer, I., Yen, A.S., and Squyres, S.W., 2010, Identification of carbonate-rich outcrops on Mars by the Spirit rover: Science, v. 329, p. 421–424, doi:10.1126/science.1189667.

Niles, P.B., Zolotov, M.Y., and Leshin, L.A., 2009, Insights into the formation of Fe- and Mg-rich aqueous solutions on early Mars provided by the ALH 84001 carbonates: Earth and Planetary Science Letters, v. 286, p. 122–130, doi:10.1016/j.epsl.2009.06.039.

Ramsey, M.S., and Christensen, P.R., 1998, Mineral abundance determination: Quantitative deconvolution of thermal emission spectra: Journal of Geophysical Research, v. 103, p. 577–596, doi:10.1029/97JB02784.

Ruff, S. W., Christensen, P. R., Blaney, D. L., Farrand, W. H., Johnson, J. R., Michalski, J. R., Moersch, J. E., Wright, S. P., and Squyres, S. W., 2006, The rocks of Gusev Crater as viewed by the Mini-TES instrument: Journal of Geophysical Research, v. 111, no. E12S18, doi:10.1029/2006JE002747.